Materials Research Bulletin 89 (2017) 286–291

Contents lists available at ScienceDirect

Materials Research Bulletin

journal homepage: www.elsevier.com/locate/matresbu

Influence of anatase titania nanoparticles content on optical and structural properties of amorphous silica

Bandar Ali Al-Asbahi[a,b,c,*]

[a] Department of Physics & Astronomy, College of Science, King Saud University, Riyadh, Saudi Arabia
[b] Department of Physics, Faculty of Science, Sana'a University, Sana'a, Yemen
[c] Research Chair in Laser Diagnosis of Cancers, College of Science, King Saud University, Riyadh, Saudi Arabia

ARTICLE INFO

Article history:
Received 4 September 2016
Received in revised form 8 December 2016
Accepted 6 January 2017
Available online 16 January 2017

Keywords:
SiO_2/TiO_2
Nanocomposite
Optical properties
Structural properties
Crystallite size

ABSTRACT

In this work, the influence of TiO_2 NPs content on optical and structural properties of amorphous SiO_2 is investigated. Amorphous SiO_2/TiO_2 thin films were wet-mixed and then deposited onto glass substrate by spin coating technique. The homogeneity distribution of anatase titania nanoparticles within amorphous silica matrix was evidenced by the results of X-ray diffraction (XRD), Raman spectroscopy, Fourier transform infrared spectroscopy (FT-IR), and field emission scanning electron microscope (FE-SEM). The crystallite size of the mixed phase increased significantly upon increment of TiO_2 NPs content. The results of emission and photoluminescence excitation (PLE) confirmed the defects creation in the SiO_2 matrix. The trapped electrons and the presence of oxygen vacancies at the TiO_2/SiO_2 interface enhanced the emission intensity of SiO_2/TiO_2 nanocomposite thin films.

1. Introduction

Nowadays, TiO_2/SiO_2 nanocomposites attract lots of attention due to its special features such as high surface acidity, large surface area, great surface hydroxyl, and improved light harvest. These features are appropriate for achieving self-cleaning performance or high photocatalytic activity [1–6]. Based on TiO_2/SiO_2 composite microstructure, it can be classified into two types namely, core–shell structure and uniform SiO_2 distribution. The interface area of the first type of TiO_2/SiO_2 composite microstructure is limited, where the preparation of a shell protected TiO_2 catalyst is normally adopted [7,8]. In contrast, the interface area of the second type between SiO_2 and TiO_2 can be increased, as recently reported, by immersing mesoporous titania microspheres in SiO_2 sol and then conducting a calcination process [9].

SiO_2/TiO_2 composite in the gel network is popularly known as an active catalysts due to the distinguish mesoporosity. By the combination of titania into silica systems/nanoparticles, it can remarkably modified the pore structure [10]. Compared to SiO_2, TiO_2 can achieve strong scattering because of its interesting properties like a higher refractive index and smaller band gap. Furthermore, once the structured clusters are indiscriminately incorporated in the optical films the incorporation of TiO_2 into the composite system led to achieve strong multiple scattering [11,12]. To synthesize metal oxide nanocomposites there are several approaches such as sol–gel method [13–15], micro-emulsion [16], hydrothermal [17], chemical coprecipitation method [18], electron beam physical vapor deposition technique [6], and radio frequency magnetron sputtering [19–23]. At low temperatures, the sol–gel technique is widely accepted as the technique to prepare a homogeneous, densified, and porous material. In addition, the controllability of such prepared material can be achieved as well.

Despite the features of potential industrial usage and easy handling of SiO_2/TiO_2 nanocomposites in the powder form, homogeneous distribution of nanoparticles in the mixed systems for chemical/optoelectronic nanostructures is required. To verify this issue as well as to produce nanocomposite materials with large surface area, unique physical modification will be reported in this work. Prior to disperse the powder of nanoparticles in ethanol solvent, small percentage volume ratio of ethylene glycol was added. Despite of the physical interaction between SiO_2 NPs and TiO_2 NPs, unique distribution for both SiO_2 and TiO_2 NPs was achieved in this work. The homogeneity of the prepared SiO_2, TiO_2, and SiO_2/TiO_2 nanocomposite thin films was evidenced by the optical and structural characterizations.

In the current work, the powder form of SiO_2 NPs was synthesized by sol-gel method. Little amount of ethylene glycol

* Corresponding author at: Department of Physics & Astronomy, College of Science, King Saud University, Riyadh, Saudi Arabia.
E-mail addresses: alasbahibandar@gmail.com, balasbahi@ksu.edu.sa (B.A. Al-Asbahi).

http://dx.doi.org/10.1016/j.materresbull.2017.01.004
0025-5408/

(EG) was added into each solution of SiO_2 NPs and TiO_2 NPs to get unique homogeneous distribution of these NPs. Prior to spin coating technique, the solution blending method was employed to prepare SiO_2/TiO_2 nanocomposites with various weight ratios. The influence of the TiO_2 NPs content on the structural and optical properties of prepared SiO_2/TiO_2 thin films at room temperature was investigated in detail.

2. Experimental procedures

2.1. Thin films preparation

SiO_2 NPs in amorphous form, with an average diameter of about 26.4 nm, were synthesized using sol-gel method as reported in the earlier published work [24]. Once the gel centrifuged and washed with ethanol and distilled water, it was calcinated at intermediate temperature for elimination of the residual organic element. Anatase TiO_2 powder (mean size of 25 nm), purchased from Sigma Aldrich, USA, have been used in this investigation. Each of SiO_2 NPs and TiO_2 NPs were dispersed separately into ethanol with 2 vol.% of ethylene glycol (EG). The liquids of both SiO_2 and TiO_2 NPs were stirred separately at 600 rpm for 2 h and then sonicated for 1 h to obtain homogenous samples. SiO_2/TiO_2 nanocomposites with different weight ratios of TiO_2 NPs (5, 10, 15, 20, 25, 30, and 35 wt.%) were prepared by solution blending method. All samples were deposited onto a glass substrate using spin coating technique (2000 rpm for 20 s) and then annealed at 120 °C in vacuum oven to remove the solvents. The films thickness for each sample was at around 230 nm, as evidenced by FE-SEM cross section images (not shown here).

2.2. Thin films characterization

The structural properties of the thin films were characterized by X-ray diffraction (XRD, Bruker-AXS D8, λ = 1.5418 Å), field emission scanning electron microscope (FE-SEM, ZEISS Supra 55VP), Raman spectroscopy (Bruker RFS 100/S,) with Nd:YAG excitation laser operating at 1064 nm and $\pm 8\ cm^{-1}$ resolution, and Fourier transform infrared spectroscopy (FT-IR, Spectrum 400 Perki-nElmer) in the range of 4000–300 cm^{-1} and at resolution of $\pm 1\ cm^{-1}$. UV–vis Spectrophotometer (Edinburg FLS920), with an excitation wavelength fixed at 300 nm, excitation slit at 10 nm, and emission slit at 15 nm, was employed to characterize the optical properties of the samples.

3. Results and discussion

3.1. X-ray diffraction

X-ray diffraction patterns of pristine SiO_2 NPs, pristine TiO_2 NPs, and SiO_2 NPs mixed with different TiO_2 NPs content (5, 10, 15, 20, 25, 30, and 35 wt.%) are illustrated in Fig. 1. The very broad hump of SiO_2 is assigned to its amorphous nature and indicated of short range ordering of Si atoms [25]. Although the dominant phase of SiO_2 is amorphous, the weak patterns (100) and (200) are indicated to existence the crystalline phase in the prepared SiO_2 which is in a good agreement with recent report [26]. However, once TiO_2 mixed into SiO_2, the diffraction patterns of anatase TiO_2 NPs were appeared in the SiO_2/TiO_2 thin films. The diffraction patterns at 25°, 38°, 48°, and 55° were assigned to the typical patterns of (1 0 1), (0 0 4), (2 0 0), and (2 0 4) of crystalline planes in anatase TiO_2 NPs, respectively. It can be clearly observed that the broadening hump was dropped as the TiO_2 content increased. The inhibition of the hump peak upon increment TiO_2 NPs can be attributed mostly to the increase in the crystallite size (D), which was calculated using

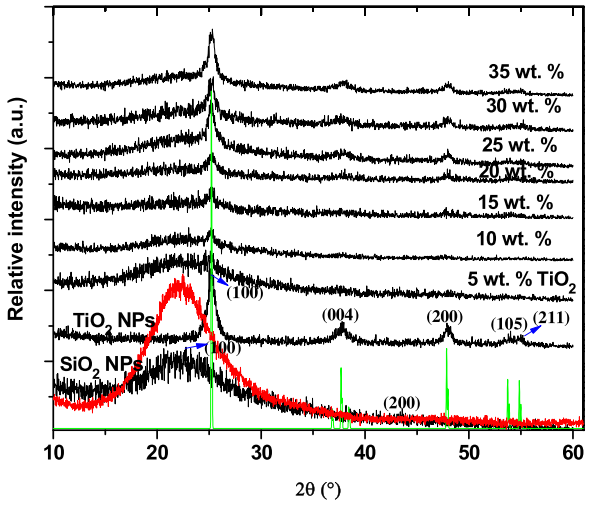

Fig. 1. X-ray diffraction patterns of SiO_2 NPs, TiO_2 NPs, and SiO_2/diff. wt.% TiO_2 nanocomposite thin films. The red and green patterns related to standard XRD patterns of SiO_2 and TiO_2, respectively.(For interpretation of the references to colour in this figure legend, the reader is referred to the web version of this article.)

Table 1
X-ray diffraction analysis for thin films of SiO_2 NPs with different weight ratios of TiO_2 NPs.

TiO_2 wt.%	FWHM	2θ (°)	Crystal size (nm)	Lattice Strain
Pure SiO_2	9.981	22.52	0.85	0.2188
15	1.226	25.22	6.94	0.0239
25	0.922	25.22	9.23	0.0180
35	0.767	25.22	11.09	0.0150
100	0.615	25.22	13.83	0.0120

Debye-Scherrer's equation and tabulated in Table 1:

$$D = \frac{0.9\lambda}{\beta\cos\theta}$$

where λ is the wavelength of X-ray beam (λ = 1.5418 Å), β is the full width at half maximum (FWHM) of the particular peak, and θ is the Braggs angle. Furthermore, there is no another distinguished crystalline phase was detected, which indicates that TiO_2 nanoparticles were highly dispersed with SiO_2 nanoparticles. The lattice strain (ε) and FWHM (ß) can be related according to the following formula [27]:

$$4\varepsilon = \beta\cos\theta$$

As shown in Table 1, it can be clearly seen significant reduction in strain upon increment TiO_2. The reduction in lattice strain can be attributed to the inverse relationship between ε and D. Moreover, in comparison with pristine TiO_2, the weak pattern peaks of SiO_2/TiO_2 nanocomposite films showed that the crystallinity was decreased. This finding may be ascribed to lattice distortion induced by interfacial strain because of the different lattice parameters between TiO_2 and SiO_2 [28].

3.2. Raman spectroscopy and FT-IR

Fig. 2 shows the Raman spectra of pristine TiO_2 NPs, pristine SiO_2 NPs, and SiO_2/TiO_2 nanocomposite thin film at high content of titania (30 wt.%). The Raman spectrum of the pristine TiO_2 NPs indicates a strong peak at 145 cm^{-1} and weak peaks at 395 cm^{-1}, 512 cm^{-1}, and 636 cm^{-1}. These peaks correspond to vibrational symmetry of E_g, B_{1g}, $A_{1g} + B_{1g}$, and E_g respectively, which are in good agreement with recent reports for anatase phase [29–31]. The

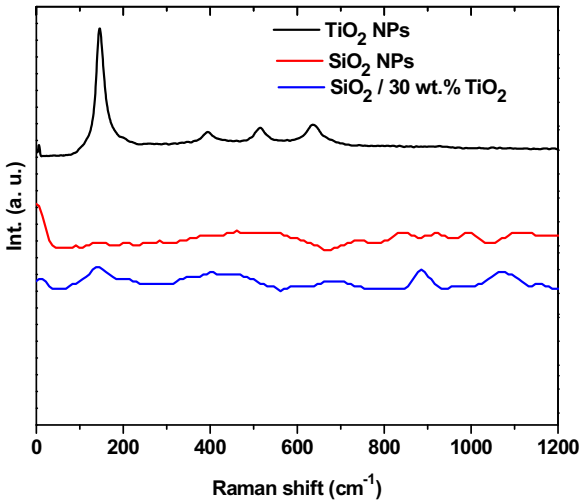

Fig. 2. Raman spectra of SiO_2 NPs, TiO_2 NPs, and SiO_2/30 wt.%TiO_2 nanocomposite thin films.

Raman spectrum of pristine SiO_2 thin film exhibits intense broad peak at the range of 330–660 cm^{-1}, and weak peaks near 840 cm^{-1}, 993 cm^{-1}, and 1100 cm^{-1}. These peaks can be attributed to bending of O—Si—O, Si—O—Si symmetric bond stretching, stretching mode of Si—OH, and asymmetric bond stretching mode of Si—O—Si [29,32]. The Raman spectrum of the SiO_2/30 wt.% TiO_2 nanocomposite exhibited a decrease in the strongest intensity peak of titania while other peaks were inhibited. This is can be attributed to the highly dispersed of titania within silica matrix hence suggesting the absence of the bulk titania formation. Moreover, the slightly blue shift of the peak at 145 cm^{-1} can be attributed to the existence of a specific kind of nonstoichiometric defects [33].

The surface chemical structure of all the thin films was investigated by FT-IR analysis (Fig. 3). In Fig. 3(a), the vibrational bands at 3350 cm^{-1} and 1640 cm^{-1} are assigned to the stretching vibration of O—H group and bending modes of adsorbed water, respectively [32], while the overlapped intense peaks at the band range 400–700 cm^{-1} are corresponding to the symmetric stretching of Ti—O—Ti [34]. The vibrational bands at 1090, 960, 802, and 462 cm^{-1} are assigned to asymmetric stretching of Si—O—Si, stretching modes of Si—OH, symmetric stretching vibration of Si—O—Si, and bending modes of Si—O—Si, respectively [35]. These observations are in good agreement with previous Raman spectra results. Moreover, as shown in Fig. 3(b), all peaks of TiO_2 and SiO_2 have been found in all samples spectra of SiO_2/TiO_2 nanocomposite thin films which confirmed the homogeneity of the nanocomposite thin films prepared even for TiO_2 NPs content as high as 35 wt.%.

3.3. FE-SEM

Fig. 4 displays the FE-SEM images of SiO_2/TiO_2 nanocomposite thin films for different content (5, 10, 20, and 30 wt.%) of TiO_2 NPs under the same scale. These images displayed the existence of silica and titania, with lighter spots corresponding to titania and darker spots to silica. This observation shows that the nanometric TiO_2 particles and SiO_2 particles are physically combined and also closely connected with each other which might also improve optical properties of the nanocomposite thin films. In addition, it can be clearly seen that the porosity of the film increases upon increment TiO_2 NPs. This finding can be also attributed to the spaces increment and increasing of particle size distribution between SiO_2 and TiO_2. Moreover, the FE-SEM images

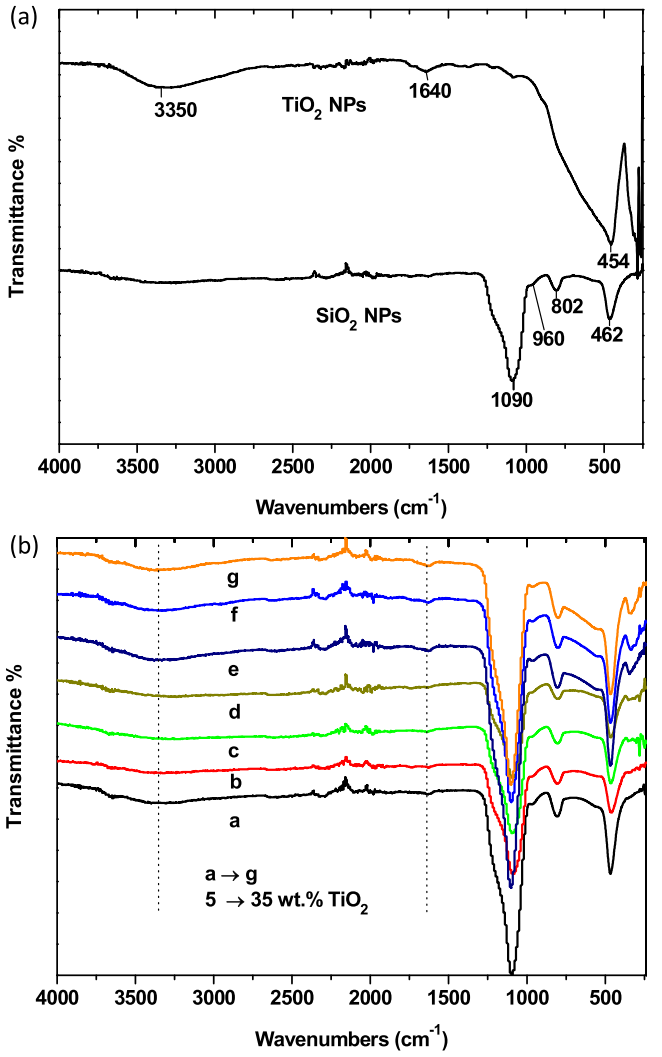

Fig. 3. FTIR spectra of (a) SiO_2 and TiO_2 NPs thin films. (b) SiO_2/diff. wt.% TiO_2 nanocomposite thin films.

demonstrated that the distribution of TiO_2 NPs was observed to be homogent even for high content of TiO_2 NPs. This observation is corroborated with previous findings of X-ray diffraction, Raman spectra, and FT-IR.

3.4. Photoluminescence analysis

Fig. 5 demonstrated the photoluminescence spectra of pristine SiO_2 NPs, pristine TiO_2 NPs, and SiO_2/TiO_2 nanocomposite thin films with various content of TiO_2 NPs. The broad emission band at 360–500 nm is attributed to TiO_2 nanoparticles which is corroborated with previous reports [36,37]. In these spectra, the main broad emission peak demonstrated at 372 nm which can be attributed to the oxygen related defects in the thin films of SiO_2/TiO_2 nanocomposite. It can be clearly noted that there is a significant increase in UV and visible emission intensities with increment of TiO_2 content. As TiO_2 NPs are well dispersed in the matrix, more holes or electrons are excited and radiative recombination of excitons increases. Consequently, the emission intensities can be enhanced significantly. However, the presence of higher amount of TiO_2 NPs led to gradual increment in crystallite size (as evidenced from the previous XRD analysis) and thus reduction in non-saturated ions and defects [38]. Consequently, the emission intensity showed reduction trend with higher TiO_2

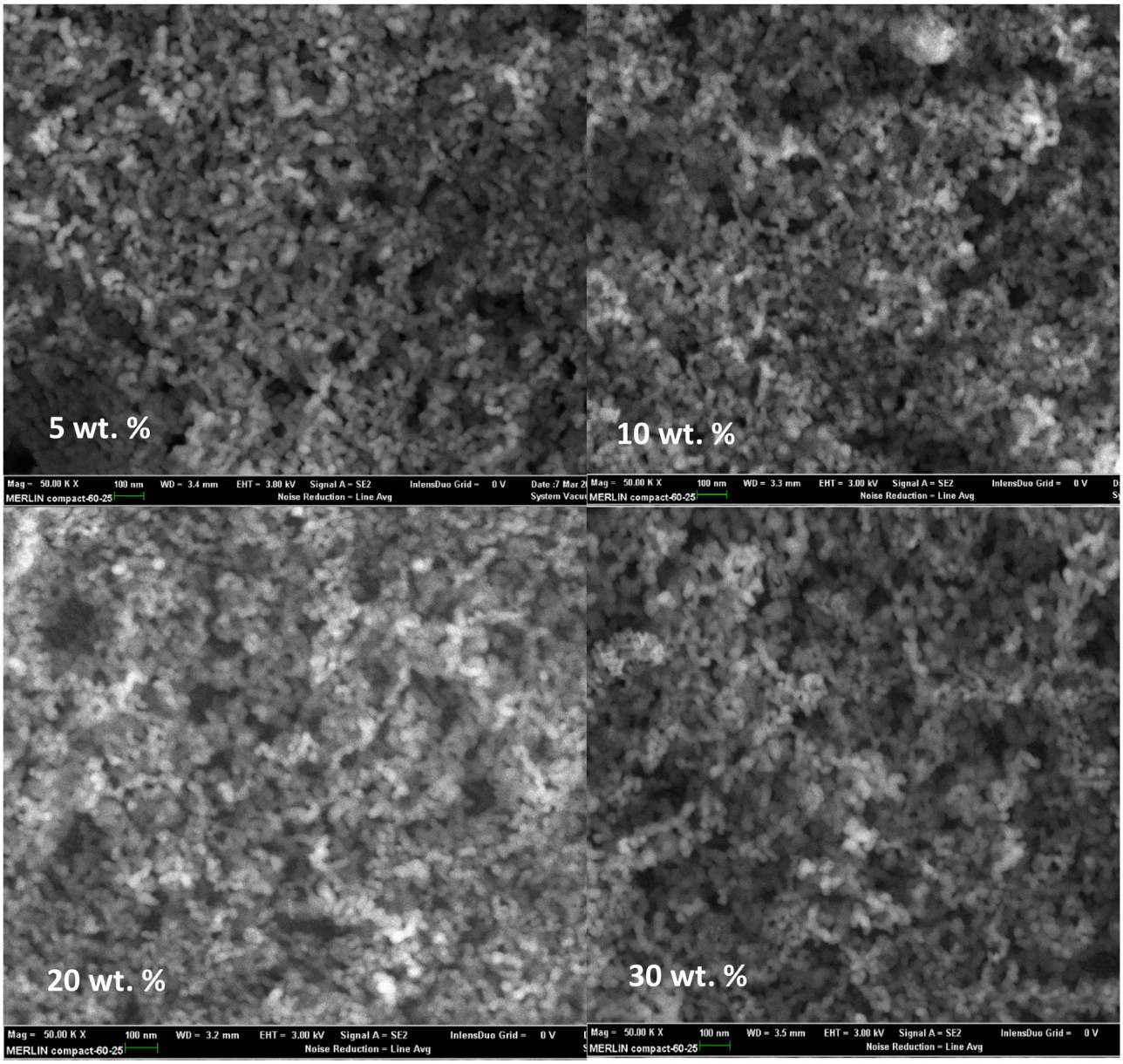

Fig. 4. FE-SEM images of SiO_2/diff. wt.% TiO_2 nanocomposite thin films.

content. Among of all the nanocomposite thin films, the sample with 5 wt.% of TiO_2 NPs exhibited the highest emission intensity. This is attributed to the abundance defects, which came from SiO_2 NPs, compared to other nanocomposite samples. At high content of TiO_2 NPs, surface states such as dangling bonds subscribe to the non-radiative processes. The enhancement in the intensity of UV emission might be attributed to the decrease of dangling bonds with reduction of TiO_2 NPs. It was confirmed from X-ray diffraction analysis that strain is performing on the SiO_2 NPs as the TiO_2 NPs content is induced. It was concluded that optimum intensity of UV emission can be achieved when the excitation wavelength chosen from the photoluminescence excitation (PLE) spectrum [39]. Fig. 6 illustrated that the main peaks of PLE spectrum of SiO_2 NPs observed at 275 nm and 284 nm, whereas it shown at 284 nm and 342 nm for SiO_2/TiO_2 thin films. The main peaks of SiO_2 NPs reduced upon increment TiO_2 NPs. The peak at 275 nm is resulted from the non-bridging oxygen hole centers [40], which are generated from the single silanol groups (Si—OH).

The mechanism of enhancement of the UV emission intensity is illustrated in Fig. 7. The band gap for SiO_2 is 10.5 eV with non-bridged oxygen and 3.03 eV for TiO_2. The higher crystallinity of the samples upon increment the TiO_2 content and the larger radius of titanium ions than silicon ions could cause little distortion in the silica-rich matrix or in the SiO_2/TiO_2 network [38]. As a result, some energy levels under 3 eV may be created in the distorted SiO_2/TiO_2. The trapped electrons at the non-bridging oxygen hole centers transfer to both conduction band (CB) of TiO_2 and the generated levels which are slightly below it. These transitions lead to enhance the emission intensity of the SiO_2/TiO_2 nanocomposite. Moreover, as the TiO_2 NPs content is increased, a lot of carriers will be available in both CB of TiO_2 and the generated levels. These carriers with the excited carriers in SiO_2 lead to more number of radiative transitions to valence band (VB) of TiO_2 and thus enhance the UV emission intensity of SiO_2/TiO_2 nanocomposites. Additionally, the enhancement in the visible emission of the samples generally resulted from the oxygen vacancies at the interface of TiO_2 [41].

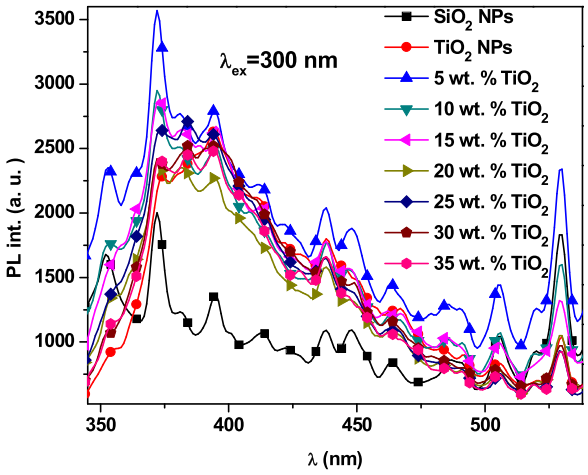

Fig. 5. Photoluminescence spectra of SiO_2 NPs, TiO_2 NPs, and SiO_2/diff. wt.% TiO_2 nanocomposite thin films.

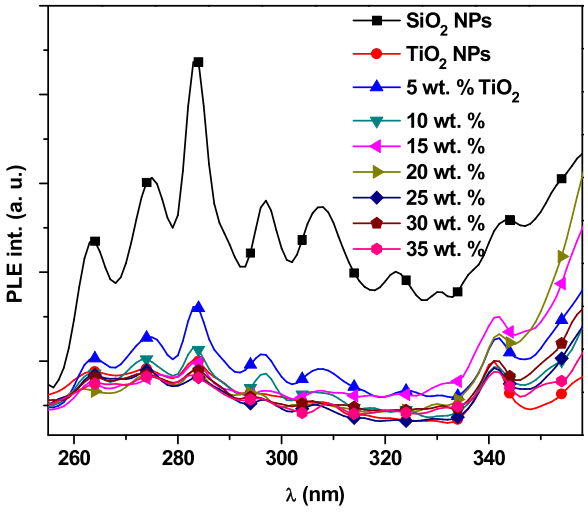

Fig. 6. Photoluminescence excitation (PLE) spectra of SiO_2 NPs, TiO_2 NPs, and SiO_2/diff. wt.% TiO_2 nanocomposite thin films.

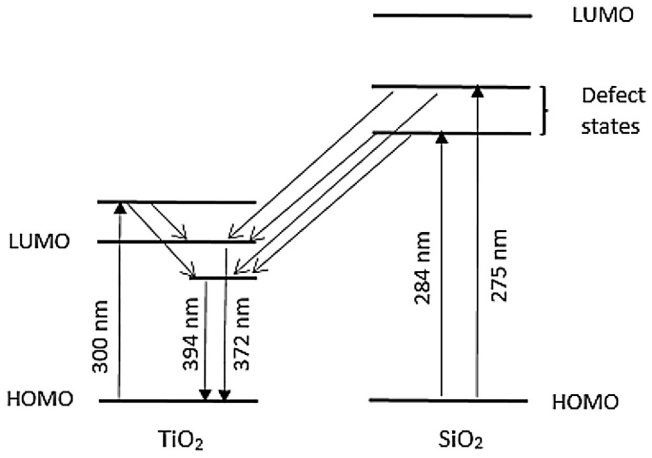

Fig. 7. Schematic mechanism of enhancement of the UV emission intensity.

4. Conclusion

The influenced of TiO_2 NPs content on optical and structural properties of SiO_2 NPs was investigated. Homogenous SiO_2/TiO_2 thin films was successfully achieved in this work. The crystallite size of TiO_2 NPs in the nanocomposite thin films was increased while its strain was decreased upon increment of TiO_2 NPs content, as indicated by the X-ray diffraction analysis. The interaction between silica and titania NPs was physically evidenced by Raman and FT-IR analysis. It is found that the optimal emission intensity of the samples was for 5 wt.% of TiO_2 NPs content, which can be attributed to abundance defects compared to other samples. The radiative transitions to the valence band (VB) of TiO_2 resulted to enhance the visible emission intensity of SiO_2/TiO_2 nanocomposites, whereas the reduction of dangling bounds resulted to improve the UV emission intensity.

Acknowledgment

This project was financially supported by King Saud University, Vice Deanship of Research Chairs.

References

[1] F. Deng, Y. Liu, X. Luo, S. Wu, S. Luo, C. Au, R. Qi, Sol-hydrothermal synthesis of inorganic-framework molecularly imprinted TiO2/SiO2 nanocomposite and its preferential photocatalytic degradation towards target contaminant, J. Hazard. Mater. 278 (2014) 108–115.
[2] C. Kapridaki, L. Pinho, M.J. Mosquera, P. Maravelaki-Kalaitzaki, Producing photoactive, transparent and hydrophobic SiO2-crystalline TiO2 nanocomposites at ambient conditions with application as self-cleaning coatings, Appl. Catal. B 156–157 (2014) 416–427.
[3] J. Wang, C. Lu, J. Xiong, Self-cleaning and depollution of fiber reinforced cement materials modified by neutral TiO2/SiO2 hydrosol photoactive coatings, Appl. Surf. Sci. 298 (2014) 19–25.
[4] M. Mazur, D. Wojcieszak, D. Kaczmarek, J. Domaradzki, S. Song, D. Gibson, F. Placido, P. Mazur, M. Kalisz, A. Poniedzialek, Functional photocatalytically active and scratch resistant antireflective coating based on TiO2 and SiO2, Appl. Surf. Sci. 380 (2016) 165–171.
[5] A. Pal, T.K. Jana, K. Chatterjee, Silica supported TiO2 nanostructures for highly efficient photocatalytic application under visible light irradiation, Mater. Res. Bull. 76 (2016) 353–357.
[6] A. Eshaghi, A.A. Aghaei, A. Eshaghi, Photocatalytic and self-cleaning properties of SiO2/TiO2/SiO2 nanostructured thin film, Int. J. Mater. Res. 104 (2013) 1263–1266.
[7] R. Tang, T. Chen, Y. Chen, Y. Zhang, G. Wang, Core-shell TiO2@SiO2 catalyst for transesterification of dimethyl carbonate and phenol to diphenyl carbonate, Chin. J. Catal. 35 (2014) 457–461.
[8] N. Guo, Y. Liang, S. Lan, L. Liu, G. Ji, S. Gan, H. Zou, X. Xu, Uniform TiO_2–SiO_2 hollow nanospheres: synthesis, characterization and enhanced adsorption–photodegradation of azo dyes and phenol, Appl. Surf. Sci. 305 (2014) 562–574.
[9] S.F. Resende, E.H.M. Nunes, M. Houmard, W.L. Vasconcelos, Simple sol–gel process to obtain silica-coated anatase particles with enhanced TiO_2-SiO_2 interfacial area, J. Colloid Interface Sci. 433 (2014) 211–217.
[10] K. Sinkó, Influence of chemical conditions on the nanoporous structure of silicate aerogels, Materials 3 (2010) 704–740.
[11] H. Zhang, X. Quan, S. Chen, H. Zhao, Fabrication and characterization of silica/titania nanotubes composite membrane with photocatalytic capability, Environ. Sci. Technol. 40 (2006) 6104–6109.
[12] N.I. Ermokhina, V.A. Nevinskiy, P.A. Manorik, V.G. Ilyin, N.N. Shcherbatyuk, D. O. Klymchyuk, A.M. Puziy, Synthesis of large-pore mesoporous nanocrystalline TiO2 microspheres, Mater. Lett. 75 (2012) 68–70.
[13] S. Islam, R.A. Rahman, Z. Othaman, S. Riaz, M. Saeed, S. Naseem, Preparation and characterization of crack-free sol–gel based SiO_2–TiO_2 hybrid nanoparticle film, J. Solgel Sci. Technol. 68 (2013) 162–168.
[14] S. Riaz, S. Naseem, Controlled nanostructuring of TiO_2 nanoparticles: a sol–gel approach, J. Solgel Sci. Technol. 74 (2015) 299–309.
[15] A. Eshaghi, A. Eshaghi, Preparation and hydrophilicity of TiO2 sol–gel derived nanocomposite films modified with copper loaded TiO2 nanoparticles, Mater. Res. Bull. 46 (2011) 2342–2345.
[16] M.H. Razali, R. Ca, W. Khairul, Modification and performances of TiO2 photocatalyst towards degradation of paraquat dichloride, J. Sustain. Sci. Manage. 8 (2013) 244–253.
[17] Z. Li, B. Hou, Y. Xu, D. Wu, Y. Sun, Hydrothermal synthesis, characterization, and photocatalytic performance of silica-modified titanium dioxide nanoparticles, J. Colloid Interface Sci. 288 (2005) 149–154.
[18] R. Singh, B. Yadav, Synthesis and characterization of copper doped tin oxide for humidity sensing applications, Adv. Sci. Lett. 20 (2014) 895–902.

[19] F. Meng, Z. Sun, A mechanism for enhanced hydrophilicity of silver nanoparticles modified TiO2 thin films deposited by RF magnetron sputtering, Appl. Surf. Sci. 255 (2009) 6715–6720.
[20] F. Meng, F. Lu, Pure and silver (2.5–40vol%) modified TiO2 thin films deposited by radio frequency magnetron sputtering at room temperature: surface topography, energy gap and photo-induced hydrophilicity, J. Alloys Compd. 501 (2010) 154–158.
[21] F. Meng, Z. Sun, Enhanced photocatalytic activity of silver nanoparticles modified TiO2 thin films prepared by RF magnetron sputtering, Mater. Chem. Phys. 118 (2009) 349–353.
[22] F. Meng, L. Xiao, Z. Sun, Thermo-induced hydrophilicity of nano-TiO2 thin films prepared by RF magnetron sputtering, J. Alloys Compd. 485 (2009) 848–852.
[23] F. Meng, X. Song, Z. Sun, Photocatalytic activity of TiO2 thin films deposited by RF magnetron sputtering, Vacuum 83 (2009) 1147–1151.
[24] M.H.H. Jumali, B.A. Al-Asbahi, C.C. Yap, M.M. Salleh, M.S. Alsalhi, Optical properties of poly (9, 9-di-n-octylfluorenyl-2.7-diyl)/amorphous SiO2 nanocomposite thin films, Sains Malays. 42 (2013) 1151–1157.
[25] Shabnam, C.R. Kant, P. Arun, Controlling the photoluminescence of ZnO:Si nano-composite films by heat-treatment, Mater. Res. Bull. 45 (2010) 1368–1374.
[26] M. Zainuri, Synthesis of SiO2 nanopowders containing quartz and cristobalite phases from silica sands, Mater. Sci-Poland 33 (2015) 47–55.
[27] B. Cullity, Element of X-Ray Diffraction, Addition–Wesley, Reading, MA, 1978.
[28] Z. Fan, F. Meng, J. Gong, H. Li, Y. Hu, D. Liu, Enhanced photocatalytic activity of hierarchical flower-like CeO2/TiO2 heterostructures, Mater. Lett. 175 (2016) 36–39.
[29] R. Peng, S. Banerjee, G. Sereda, R.T. Koodali, TiO2–SiO2 mixed oxides: organic ligand templated controlled deposition of titania and their photocatalytic activities for hydrogen production, Int. J. Hydrogen Energy 37 (2012) 17009–17018.
[30] T. Ohsaka, Temperature dependence of the raman spectrum in anatase TiO2, J. Phys. Soc. Jpn. 48 (1980) 1661–1668.
[31] Z. Fan, F. Meng, J. Gong, H. Li, A. Li, Growth mechanism and photocatalytic activity of chrysanthemum-like anatase TiO2 nanostructures, Ceram. Int. 42 (2016) 6282–6287.
[32] K.S. Babu, A.R. Reddy, K.V. Reddy, Controlling the size and optical properties of ZnO nanoparticles by capping with SiO2, Mater. Res. Bull. 49 (2014) 537–543.
[33] Z. Fan, F. Meng, M. Zhang, Z. Wu, Z. Sun, A. Li, Solvothermal synthesis of hierarchical TiO2 nanostructures with tunable morphology and enhanced photocatalytic activity, Appl. Surf. Sci. 360 (2016) 298–305.
[34] X. Bu, Y. Zhou, M. He, Z. Chen, T. Zhang, Optically active SiO2/TiO2/polyacetylene multilayered nanospheres: preparation, characterization, and application for low infrared emissivity, Appl. Surf. Sci. 288 (2014) 444–451.
[35] K.Y. Jung, S.B. Park, Enhanced photoactivity of silica-embedded titania particles prepared by sol–gel process for the decomposition of trichloroethylene, Appl. Catal. B 25 (2000) 249–256.
[36] Y. Lei, L.D. Zhang, Fabrication, characterization, and photoluminescence properties of highly ordered TiO2 nanowire arrays, J. Mater. Res. 16 (2001) 1138–1144.
[37] W.H. Green, K.P. Le, J. Grey, T.T. Au, M.J. Sailor, White phosphors from a silicate-carboxylate sol-gel precursor that lack metal activator ions, Science 276 (1997) 1826–1828.
[38] C.F. Song, M.K. Lü, P. Yang, D. Xu, D.R. Yuan, Structure and photoluminescence properties of sol–gel TiO2–SiO2 films, Thin Solid Films 413 (2002) 155–159.
[39] K. Sowri Babu, A. Ramachandra Reddy, C. Sujatha, K. Venugopal Reddy, Optimization of UV emission intensity of ZnO nanoparticles by changing the excitation wavelength, Mater. Lett. 99 (2013) 97–100.
[40] J.E. Van Nostrand, R. Cortez, Z.P. Rice, N.C. Cady, M. Bergkvist, Local transport properties, morphology and microstructure of ZnO decorated SiO2 nanoparticles, Nanotechnology 21 (2010) 415602.
[41] B.J. Jin, S. Im, S.Y. Lee, Violet and UV luminescence emitted from ZnO thin films grown on sapphire by pulsed laser deposition, Thin Solid Films 366 (2000) 107–110.